Chinese Chemical Letters 35 (2024) 109153

Contents lists available at ScienceDirect

Chinese Chemical Letters

journal homepage: www.elsevier.com/locate/cclet

Activatable photoacoustic bioprobe for visual detection of aging *in vivo*

Zihong Li, Jie Cheng, Ping Huang, Guoliang Wu, Weiying Lin*

Institute of Optical Materials and Chemical Biology, Guangxi Key Laboratory of Electrochemical Energy Materials, School of Chemistry and Chemical Engineering, Guangxi University, Nanning 530004, China

ARTICLE INFO

Article history:
Received 4 July 2023
Revised 22 September 2023
Accepted 25 September 2023
Available online 5 October 2023

Keywords:
Near-infrared
Photoacoustic
Aging
Senescence
Tumor
Sa-β-gal

ABSTRACT

Aging is a natural physiological process with various challenges, related to the loss of homeostasis within the organism, which is not a disease, but a significantly strong risk factor for multiple diseases, including myocardial infarction, stroke, some age-related cancers, macular degeneration, osteoarthritis, neurodegeneration, and many others. In the body, the main manifestation of aging is cellular aging, which exists within tissues and has a local or global impact on tissue function. However, the lack of effective aging detection tools has always been an issue that cannot be ignored in the field of aging research. Therefore, it is necessary to construct a non-invasive tool for *in vivo* detection of aging. Here, we show that the photoacoustic probe (**LGAL**), which has peak excitation and emission wavelengths in the near-infrared optical window, binds *in vivo* and at high contrast to the hallmark of aging, and allows for the microscopic imaging of aging through the intact mice. Firstly, this tool **LGAL** has been successfully applied to detect senescence in cells, displaying stronger photoacoustic signals than normal cells. Then, by using the photoacoustic probe, the blood vessels and tissues inside the mice can be visualized. Young and elderly mice exhibit varying intensities of photoacoustic signals, marking the first time a probe has been used to explore the aging of blood vessels and tissues inside the mice. Finally, we monitored the changes in the degree of aging during tumor treatment under photoacoustic (PA) imaging for the first time. As the treatment time increased, the degree of aging of the tumor gradually deepened. We expect the powerful tool could be a noninvasive and powerful tool for the study of aging biology.

Aging, we broadly define it as a time related functional decline that affects most organisms [1]. Aging is a natural physiological process with various challenges, related to the loss of homeostasis within the organism, and often has negative effects on health [2,3]. It will become a reality to achieve health and longevity by deeply exploring aging and preventing age-related diseases [4]. Aging is not a disease, but a significantly strong risk factor for multiple diseases, including myocardial infarction, stroke, some age-related cancers, macular degeneration, osteoarthritis, neurodegeneration, and many others [5–7]. Aging biology is an active and rapidly developing field in biomedical research [8,9]. For many years, it has been dedicated to the study of aging, and the progress made in understanding the key role of aging as a risk factor for chronic diseases has provided impetus for these studies [10–13]. The primary manifestation of aging is cellular senescence [14]. In the body, senescence cells exist within tissues, and their impact on tissue function can be local or global [15–17]. However, the lack of effective tools for detecting aging has always been an issue that cannot be ignored in the field of aging research. Thus, to enable better study aging progression in human and mouse models, there is an urgent need to develop improved methods for non-invasive imaging of biomarker in the living body. As a marker of senescent cells, senescence-related beta-galactosidase (SA-β-gal) is the gold standard for aging [18–20]. Thus, measuring SA-β-gal activity has become a simple and easy method to detect aging.

Molecular probes have low toxicity, noninvasive and membrane permeability, and can maintain the activity of biological samples [21]. Moreover, combined with optical imaging technology, *in-situ* visualization of target molecules in living cells and *in vivo* can be realized [22–25]. Nowadays, molecular probes play a more important role in the biomedical fields, such as disease, diagnosis, and efficacy monitoring [26–28]. It is worth noting that compared with traditional fluorescence imaging, photoacoustic imaging has attracted extensive attention in recent years. Photoacoustic (PA) imaging has attracted extensive attention over recent years, since it combines the high-contrast properties of pure optical imaging with the high penetration depth of pure ultrasound imaging, which can provide high-resolution and high-contrast tissue imaging [29,30]. The main advantage of photoacoustic imaging is that it can significantly reduce the photon absorption, scattering and self-absorption

* Corresponding author.
E-mail address: weiyinglin2013@163.com (W. Lin).

https://doi.org/10.1016/j.cclet.2023.109153
1001-8417/

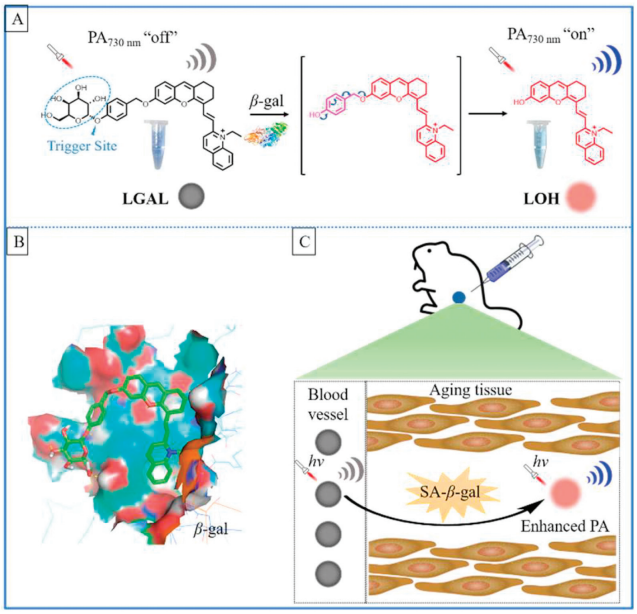

Scheme 1. Schematic illustration of the aging-responsive near infrared (NIR) PA probe **LGAL**. (A) Catalyzed mechanism of **LGAL** activated by β-gal. (B) The catalytic mechanism of **LGAL** and β-gal. (C) The probe **LGAL** is activated in the aging vessels and tissues.

of biological tissues, significantly increase the penetration depth of light in biological tissue (~5 cm), and improve the signal-to-noise ratio and spatiotemporal resolution of the imaging [31–36]. At present, there is a lack of suitable tools to detect aging *in vivo* non-invasively and effectively. In order to address this problem, the probe requires minimal tissue damage, low background interference, strong tissue penetration, and can be applied *in vivo* imaging without causing damage to the body. Therefore, it is of great significance to construct a near-infrared photoacoustic probe to study aging *in vivo*.

In this paper, to visual detecting of aging *in vivo*, we have developed an activatable near-infrared photoacoustic bioprobe. We introduce the synthesis, spectral characteristics, photoacoustic characteristics, and biological imaging of the near-infrared photoacoustic probe. Importantly, by using photoacoustic imaging, we detect aging in the living mice and the cellular senescence during the tumor's treatment was revealed.

Near-infrared dye has the advantages of low background interference, strong tissue penetration and low tissue damage [30], therefore, we used a near-infrared dye platform to develop a photoacoustic probe **LGAL**. **LGAL** combines a near-infrared dye and photoacoustic signal emission with a β-gal recognition group (galactose residue) *via* a glycosidic bond (Scheme 1A). **LGAL** should form phenolic intermediates after removing the galactose group, and then undergo a 1,6-elimination of the *p*-quinone-methide, thus producing a turn on of the photoacoustic signal. In order to confirm this conjecture, we monitored the products obtained by treatment of **LGAL** with the enzyme β-gal by mass spectrometry. A peak at *m/z* 382.1807 appears in the electrospray ionization mass spectrometry (ESI-MS), which is consistent with the molecular weight of the dye, supporting the sensing mechanism (Fig. S15 in Supporting information). Moreover, we performed molecular docking of the probe and the enzyme. As shown in Scheme 1B, **LGAL** can be efficiently docked with the enzyme, which confirms that **LGAL** should exhibit good binding with β-gal. The specific docking methods and data are shown in the supporting information. Therefore, we further synthesized and applied the probe **LGAL** at the biological level (Scheme 1C). The synthesis of probe is shown in Scheme S1 (Supporting information). The structures were confirmed using ^{1}H-nuclear magnetic resonance (NMR), ^{13}C NMR and high resolution mass spectroscopy (HRMS) (Figs. S9–S14 in Supporting information).

With the probe in hand, we evaluated the spectral response of the probe **LGAL** and β-gal (Fig. S1 in Supporting information). As shown in Fig. S1A, before β-gal was added, the absorption peak was at about 570 nm ($\varepsilon = 8.60 \times 10^3$ L mol^{-1} cm^{-1}). However, after reaction with β-gal, the peak in the UV–vis absorption spectra at 570 nm gradually decreased, and an intense signal appeared at 730 nm ($\varepsilon = 1.43 \times 10^4$ L mol^{-1} cm^{-1}), which was enhanced by about 143-fold (0–0.24 U/mL). Fig. S1B indicates a linear relationship from 0 to 0.12 U/mL with a good linear correlation ($R^2 = 0.9936$) for the probe **LGAL** and β-gal, which confirms that **LGAL** can detect β-gal of different concentrations with a detection limit of 7.075×10^{-6} U/mL. Selectivity experiments indicated that the probe **LGAL** only responded to β-gal, and did not respond to other interfering substances (CO_3^{2-}, Mn^{2+}, I^-, Na^+, Co^{2+}, K^+, Mg^{2+}, Cu^{2+}, F^-, NO_2^-, ClO^-, ACN^-, HSO_3^-, HS^-, Hcy, GSH, Cys, α-D-glucose, lysozyme, pepsin, cellulase, ·OH, H_2O_2, O_2^-, Figs. S1C and D), and the response of **LGAL** to β-gal was also very stable at physiological pH (Fig. S1E). As shown in Fig. S1F, the absorption spectrum of **LGAL** remains unchanged at different temperatures. While the response of **LGAL** to β-gal was slightly affected by temperature. At 23, 25, and 30 °C, the absorption peak at 730 nm after **LGAL** responded to β-gal slightly decreased. At 35–50 °C, the absorption peak at 730 nm after **LGAL** responded to β-gal remained basically unchanged. Generally speaking, the optimal temperature for enzymes in animals is between 35 and 40 °C. Within this range, the response of **LGAL** and β-gal is basically unaffected by temperature changes, indicating that **LGAL** responds well to β-gal in the organism. We then evaluated the kinetic behavior of **LGAL** towards β-gal (Fig. S2 in Supporting information). As shown in Fig. S2A, the reaction between **LGAL** and β-gal was complete within 12 min. We continued monitoring for 180 min and the absorption intensity remained constant, which indicated that the substance produced after the reaction was stable (Fig. S2B). Moreover, since the target molecule of the probe response was an enzyme, we used the Lineweaver-Burk equation to plot and calculate the Michaelis constant of 29.92 μmol/L, which indicated that β-gal had good affinity for the substrate **LGAL** (Figs. S2C and D). Thus, **LGAL** exhibits advantageous optical properties including low detection limits, enhanced response, excellent affinity for β-gal and rapid response.

To assess the photoacoustic performance of **LGAL**, we carried out the photoacoustic evaluation of **LGAL** with β-gal *in vitro*. Based on the spectral results for **LGAL**, we explored the photoacoustic detection of **LGAL** and β-gal using 730 nm as the excitation wavelength. As shown in Fig. 1A, before adding β-gal, the probe **LGAL** exhibited only a weak photoacoustic signal; with an increase in the amount of β-gal, the photoacoustic signal gradually increased. When the amount of β-gal reached 0.24 U/mL, the photoacoustic signal of the probe was enhanced by about 11.4 times (0–0.24 U/mL, $P < 0.0001$). In addition, we plotted the amount of β-gal and photoacoustic signal intensity (Fig. S3 in Supporting information), and calculated that the detection limit of **LGAL** was 1.36×10^{-5} U/mL. Moreover, with an increase of β-gal concentration, the color of probe **LGAL** solution gradually changed from blue-purple to blue-green, and the $PA_{730\ nm}$ signal gradually increased (Fig. 1B). Next, we evaluated the photoacoustic response of **LGAL** at different times. As shown in Fig. 1C, the photoacoustic signal of the probe increased rapidly within 0 to 10 min and leveled off after 11 min. The photoacoustic signal and visual color of the corresponding solution from 0 to 10 min changed significantly (Fig. 1D). The first-order reaction rate constant of the probe was calculated as 0.17 min^{-1} (Fig. S4 in Supporting information). The selectivity experiments of **LGAL** indicated that the photoacoustic

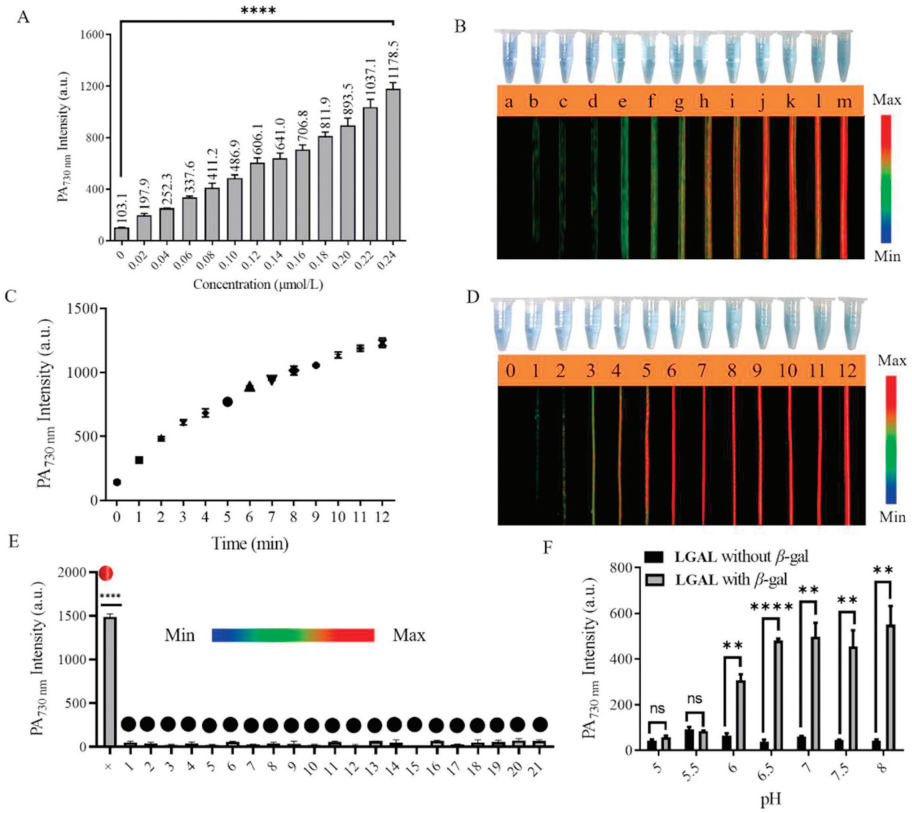

Fig. 1. The PA_{730} images of **LGAL** (20 μmol/L) to β-gal *in vitro*. (A) PA_{730} images of 20 μmol/L **LGAL** with 0–0.24 U/mL β-gal at pH 7.4. (B) The color image under natural light and corresponding PA images (λ_{ex} = 730 nm) of probe **LGAL** (20 μmol/L) upon the addition of β-gal (a, 0; b, 0.02; c, 0.04, d, 0.06; e, 0.08; f, 0.10; g, 0.12; h, 0.14; i, 0.16; j, 0.18; k, 0.20; l, 0.22; m, 0.24 U/mL). (C) PA_{730} images of 20 μmol/L **LGAL** and β-gal with time (0–12 min). (D) The color image under natural light and corresponding PA images (λ_{ex} = 730 nm) of probe. (E) PA_{730} image of **LGAL** (20 μmol/L) with β-gal (0.24 U/mL) and other interferences (1. CO_3^{2-}, 2. Mn^{2+}, 3. I^-, 4. Na^+, 5. Co^{2+}, 6. K^+, 7. Mg^{2+}, 8. Cu^{2+}, 9. F^-, 10. NO_2^-, 11. ClO^-, 12. ACN^-, 13. HSO_3^-, 14. HS^-, 15. Hcy, 16. GSH, 17. Cys, 18. α-D-glucose, 19. lysozyme, 20. pepsin, 21. cellulase). (F) PA_{730} image of 20 μmol/L **LGAL** with 0.24 U/mL β-gal at solutions with different pH. Mean ± standard deviation (SD), n = 3. ns, $P > 0.05$; $^{**}P < 0.01$, $^{****}P < 0.0001$.

signal was enhanced only when β-gal was added (Fig. 1E). Moreover, the photoacoustic signal of **LGAL** after reaction with β-gal enhanced from pH 5 to 6.5, and was then stable (pH 6.5 to 8). It is worth noting that at physiological pH (7.4), the probe **LGAL** exhibits a strong photoacoustic signal after reaction ($P < 0.01$), which was suitable for imaging applications (Fig. 1F).

Next, **LGAL** was used to image senescence in cells. Cytotoxicity experiment were performed prior to cell imaging using HeLa, B16 and 4T-1 cells that were cultured with different concentrations of **LGAL** for 24 h, respectively. MTT results indicated that the survival rate of the cells exceeded 85% (Fig. S5A in Supporting information), which confirms that **LGAL** can be imaged in living cells with little damage. Based on the good biological properties of the probe in cells and the suitable test results *in vitro*, we then explore the photoacoustic imaging ability of **LGAL** in living cells. For the experiments, two groups were prepared from the cancer cells, one of them was the normal cultured cells, which was the control group; the other group was the senescent cells obtained after cisplatin (2 μg/mL) treatment for 7 days, which was the experimental group, X-gal standard staining method confirmed the production of SA-β-gal (Fig. S6 in Supporting information).

Here, we used a low dose of cisplatin to carry out the experiment. Cells were centrifuged to obtain cell particles for imaging using a photoacoustic imaging system after incubation with **LGAL** for 30 min (Fig. S5B in Supporting information). As shown in Fig. S5C (Supporting information), the photoacoustic signal of normal cultured HeLa cells was low, while the photoacoustic signal was significantly enhanced for senescent HeLa cells with SA-β-gal expression. Furthermore, we quantified the photoacoustic signal. In normal HeLa cells, the photoacoustic intensity was 87.80, while in senescent HeLa cells, the photoacoustic intensity was 631.64, which represents an increase of about 7.2-fold (Fig. S5D in Supporting information). Statistical analysis indicated that **LGAL** could readily distinguish normal HeLa cells from senescent HeLa cells through changes of photoacoustic signal intensity ($P < 0.0001$). We then repeated the experiments with B16 cells, and for normal cells, the photoacoustic intensity of **LGAL** was 83.85, while in senescent cells with SA-β-gal expressed, the photoacoustic intensity was 619.62, which was an increase of about 7.4-fold ($P < 0.0001$, Fig. S5D). In 4T-1 cells, the imaging was consistent with the above two kinds of cells. In normal cells, the photoacoustic intensity of the probe **LGAL** was 78.93, while in senescent cells with SA-β-gal expression, the photoacoustic intensity was 621.30, which represents a signal enhancement of around 7.6-fold ($P < 0.0001$, Fig. S5D). These experimental results confirmed that **LGAL** can detect SA-β-gal in a variety of cancer cells.

Next, we explored whether the probe can be applied *in vivo*. Divide two groups, one group takes 100 μmol/L of **LGAL** (ROI 1), and the other group takes 100 μmol/L of **LGAL** and adds 0.1 U β-gal (ROI 2). We first examined the background signal of the mouse under 730 nm excitation. Then, inject the two groups of reagents into the thighs of mice on both sides (Fig. S7A in Supporting information). As shown in Fig. S7B (Supporting information), there were no photoacoustic signals on both sides of the mouse's thighs, after injecting the reagents, the signals on both sides of the mouse's thighs increased, but the photoacoustic signals in the region ROI 2 were significantly higher than those in the region ROI 1 (Fig. S7C in Supporting information), which showed that the increase of

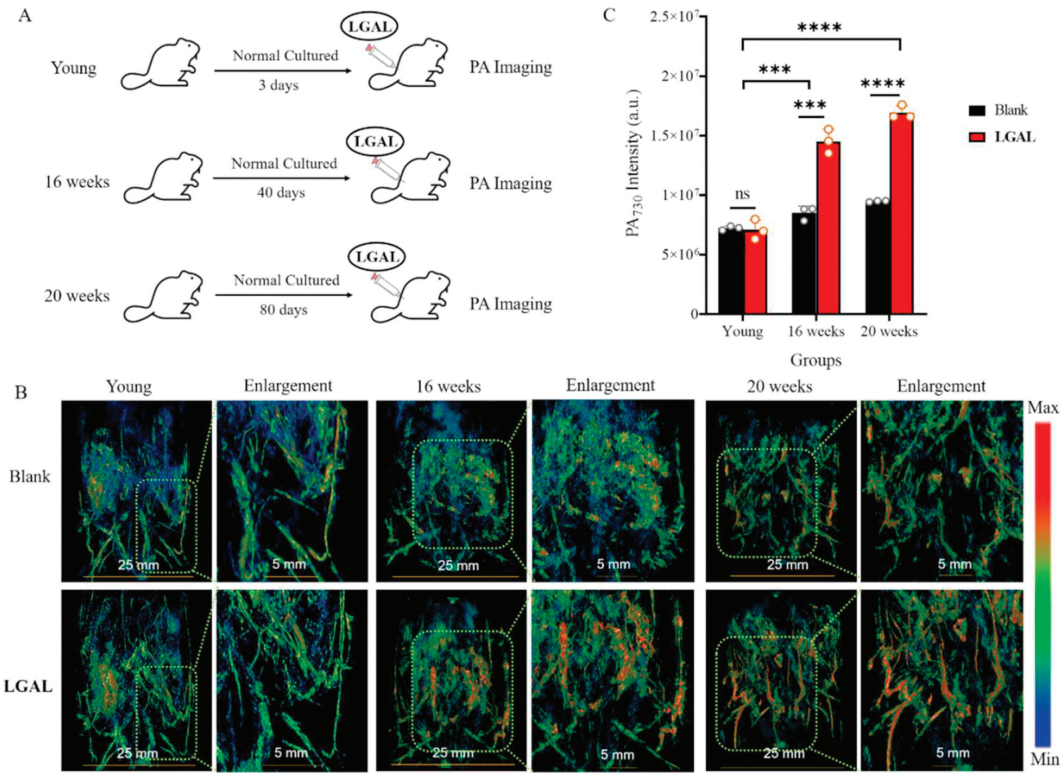

Fig. 2. Endogenous PA imaging in living mice with **LGAL**. λ_{ex} = 730 nm. (A) Model of Endogenous imaging of mice (4 weeks, young; 16 weeks; 20 weeks). (B) PA imaging of mice. (C) Image of experimental data of endogenous PA in mice. Mean ± SD, n = 3. $^{***}P < 0.001$, $^{****}P < 0.0001$.

photoacoustic signal after the probe responded to β-gal can be observed *in vivo*. Furthermore, we quantified the photoacoustic intensity of two regions, as shown in Fig. S7D (Supporting information), the photoacoustic intensity of ROI 2 increased by approximately 2.84 times compared to ROI 1 ($P < 0.0001$). The above results indicate that **LGAL** can generate photoacoustic signals for detection *in vivo*.

The excellent results of **LGAL** in exogenous imaging of senescent cells and *in vivo* inspire us to apply it to endogenous imaging of aging *in vivo*. The female mice (4–5 weeks) were obtained from the Experimental Animal Center of the Guangxi Medical University (Nanning, China). All animal experiments were reviewed and approved by the Animal Care and Experiment Committee of Guangxi University (protocol number: Gxu-2021–115). We divided mice of different ages into three groups: one group was young mice (4 weeks), and two groups were aged mice of different stages, divided into 16 and 20 weeks (Fig. 2A). Take one mouse from each group to dissect its tissue and use X-gal staining, as shown in Fig. S6B, the slices of the elderly mice are stained blue, while the young mice are colorless. Furthermore, **LGAL** was intraperitoneally injected into the mice. We continuously monitor the mice to observe the position and photoacoustic intensity of **LGAL**. As shown in Fig. S8 (Supporting information), there was a significant change in the photoacoustic intensity of blood vessels and tissues in elderly mice before and after the addition of the probe and the photoacoustic signal of **LGAL** reached its optimal observation period at 3 h. Thus, **LGAL** can be able to observe the aging status of blood vessels and abdominal tissues. As shown in Fig. 2B, the photoacoustic signal of young mice showed weak changes, while the photoacoustic signal in tissues and blood vessels remained almost unchanged (Fig. 2C, $P > 0.05$). However, the photoacoustic signal of elderly mice showed significant changes after the addition of probe **LGAL** (Fig. 2B). The photoacoustic signal intensity of mice at 16 weeks increased by about 1.70 times (Fig. 2C, $P < 0.001$), and that of mice at 20 weeks increased by about 1.81 times ($P < 0.0001$). Next, we compared the photoacoustic signals of elderly and young mice. The 16 weeks old mice showed an increase of approximately 2.06 times ($P < 0.001$) compared to young mice, while the 20 weeks old mice showed an increase of approximately 2.41 times ($P < 0.0001$) compared to young mice (Fig. 2C). The above experimental results demonstrate that the probe can detect aging *in vivo*.

Finally, we turned our attention to the use of the photoacoustic imaging system to detect aging in the tumor of mice. After 15 days, a mouse model of tumor xenotransplantation was obtained. Based on this model, we used cisplatin to treat the tumors, and monitored the changes of aging degrees of the tumor using the probe **LGAL** (Fig. 3A). Cisplatin, as an anticancer drug, can induce the aging of tumor cells. Low dose chemotherapy can make cancer cells senescent. In terms of mechanism, platinum drugs, such as cisplatin, carboplatin and oxaliplatin, cause extensive DNA damage and aging through DNA cross-linking [37]. The probe **LGAL** was injected into the tumor using intra-tumoral injection. As the above experiments showed that the probe completed its response to SA-β-gal in the body within 3 h, so after 3 h of injection of the probe, we observed the photoacoustic imaging of mice at an excitation wavelength of 730 nm. Before *in vivo* imaging, we evaluated the toxicity of the probe **LGAL** to mice. The probe **LGAL** was injected into mice through intramuscular injection. After 7 days, the mice were dissected to obtain the kidney, liver, and muscle of the injection site, and pathological sections were obtained. As shown in Fig. 3D, there was no abnormality in the organ and tissue sections of mice after injection, indicating that the toxicity of the probe **LGAL** to mice was low.

Therefore, we used the photoacoustic probe **LGAL** to detect aging in the tumors using changes of photoacoustic signals. As shown in Fig. 3B, on day 0, the photoacoustic signal of the probe **LGAL** in the tumor was very weak and was weakly enhanced compared with the blank group without the probe **LGAL** (0.056 to 0.058, $P >$

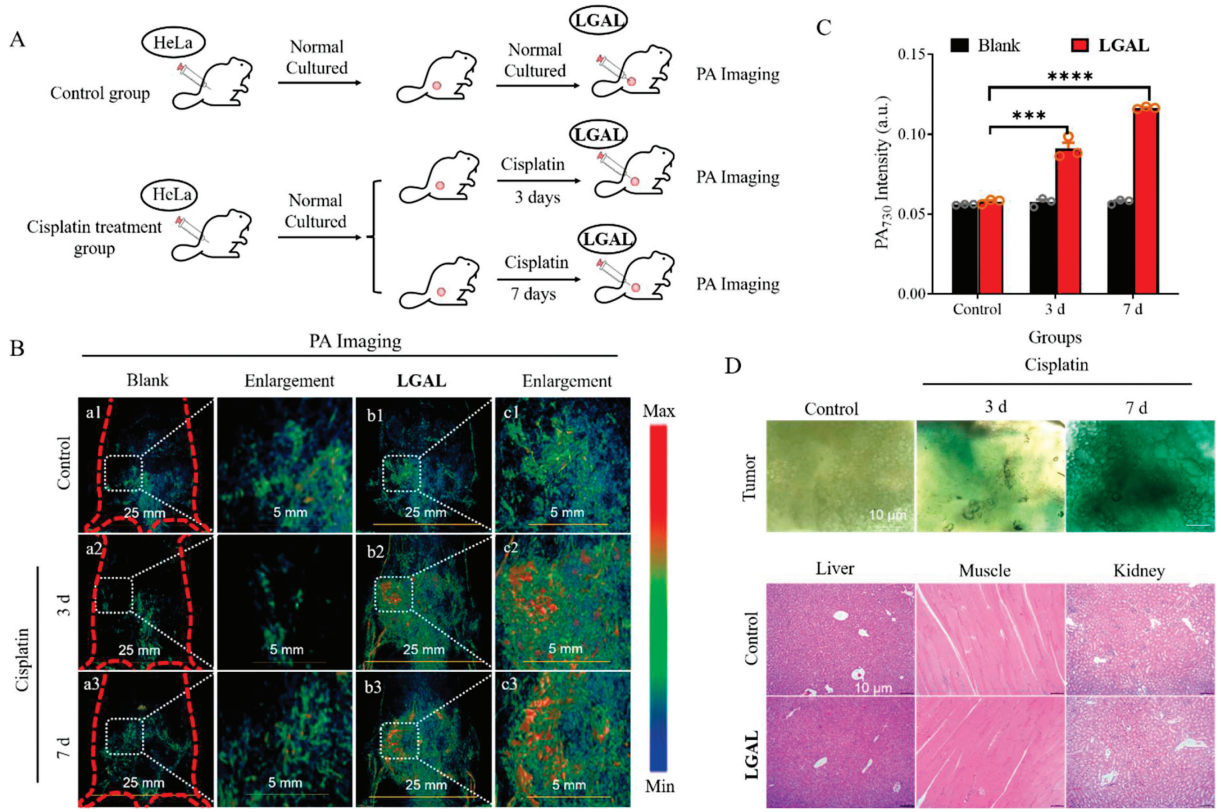

Fig. 3. PA imaging of aging in the tumors of living mice with **LGAL**. (A) Model of imaging of mouse. (B) PA imaging of the tumors of mice. (C) Image of experimental data of PA intensity in mice. (D) X-gal staining of the slices of the tumors and the histopathological results of different organs (liver, muscle of the injection site, and kidney) about control group and obese mice exposed to 100 μL 2 mmol/L **LGAL** for 7 days (magnification = ×100). λ_{ex} = 730 nm, Mean ± SD, n = 3. $^{***}P < 0.001$, $^{****}P < 0.0001$.

0.05, Fig. 3C). After 3 days of cisplatin treatment, the photoacoustic signal of **LGAL** in the tumor was significantly enhanced compared with that on day 0 (0.058 to 0.098, $P < 0.001$, Fig. 3C), which indicated that the tumor gradually aged under the stimulation of cisplatin. In addition, the photoacoustic signal increased significantly compared with the blank group without probe. After 7 days of cisplatin treatment, the photoacoustic signal of the probe **LGAL** in the tumor increased compared with that observed on day 0 (0.058 to 0.116, $P < 0.0001$, Fig. 3C) and small increasing compared with day 3, which indicated that the senescent cells in the tumor increased gradually under the stimulation of cisplatin. Moreover, the photoacoustic signal increased more strongly than that in the blank group without the probe (0.057 to 0.116, $P < 0.0001$, Fig. 3C). Therefore, the probe **LGAL** could be useful for detecting the senescence of tumor treatments through monitoring aging process, which provide a powerful tool for the development of the therapies for cancer. In addition, we used X-gal standard staining for the dissected tumor tissue blocks of tumor bearing mice treated with cisplatin for 0, 3, and 7 days to verify the validity of our experiments. The tumor tissue blocks stained with X-gal are shown in Fig. 3D. The tumor blocks obtained after 0 days of treatment exhibited no color, and those obtained after 3 days of treatment were blue, which indicated the production of SA-β-gal. The color deepened after 7 days of treatment, indicating the increase of SA-β-gal activity. Based these observations, we can used probe **LGAL** to detect aging in the tumors of mice.

In conclusion, in order to detect aging *in vivo*, we have successfully developed a new near-infrared photoacoustic probe **LGAL**, and verified its rationality through molecular docking engineering. By virtue of the probe **LGAL**, aging can be accurately detected in cells and *in vivo*. The results of the cell imaging study have indicated that the β-gal activity in the senescent cells is higher than that for normal cells. In addition, **LGAL** successfully distinguished young mice from elderly mice, displaying weak photoacoustic signals in young mice and strong photoacoustic signals in elderly mice, marking the first time a probe has been used to explore the aging of blood vessels and tissues inside the mice. It is worth noting that for the first time, we have successfully monitored the changes in the degree of aging during tumor treatment under PA imaging. The photoacoustic imaging can provide unprecedented opportunities for real-time non-invasive detection of aging at a sensitivity level and tissue depth. We hope that this study can provide a powerful tool for the study of aging biology.

Declaration of competing interest

The authors declare that they have no known competing financial interests or personal relationships that could have appeared to influence the work reported in this paper.

Acknowledgments

This work was financially supported by National Natural Science Foundation of China (Nos. 21877048, 22077048, and 22277014), Guangxi Natural Science Foundation (Nos. 2021GXNSFDA075003, AD21220061), and the startup fund of Guangxi University (No. A3040051003).

Supplementary materials

Supplementary material associated with this article can be found, in the online version, at doi:10.1016/j.cclet.2023.109153.

References

[1] C. Debes, A. Papadakis, S. Gronke, O. Karalay, L.S. Tain, et al., Nature 616 (2023) 814–821.
[2] T. Niccoli, L. Partridge, Curr. Biol. 22 (2012) 741–752.
[3] J.L. Schneider, J.H. Rowe, C. Garcia-de-Alba, et al., Cell 184 (2021) 1990–2019.
[4] A.V. Poznyak, N.K. Sadykhov, A.G. Kartuesov, et al., Int. J. Mol. Sci. 23 (2022) 13.
[5] T.W. Wang, Y. Johmura, N. Suzuki, S. Omori, et al., Nature 611 (2022) 358.
[6] A.L. Roy, F. Sierra, K. Howcroft, et al., Cell 183 (2020) 1143–1146.
[7] K. Evangelou, P.V.S. Vasileiou, A. Papaspyropoulos, et al., Physiol. Rev. 103 (2023) 40.
[8] D. Carmona-Gutierrez, A.L. Hughes, F. Madeo, C. Ruckenstuhl, Ageing Res. Rev. 32 (2016) 2–12.
[9] R. Waziry, C.P. Ryan, D.L. Corcoran, et al., Nat. Aging 3 (2023) 248–257.
[10] G.E. Neurohr, R.L. Terry, J. Lengefeld, et al., Cell 176 (2019) 1083.
[11] J. Campisi, P. Kapahi, G.J. Lithgow, et al., Nature 571 (2019) 183–192.
[12] A. Santoro, E. Bientinesi, D. Monti, Ageing Res. Rev. 71 (2021) 19.
[13] P. Hari, F.R. Millar, N. Tarrats, et al., Sci. Adv. 5 (2019) 14.
[14] S. Wang, S. Hu, Y. Mao, Aging Med. 4 (2021) 153–158.
[15] J.M. Harland, Early Mediev. Eur. 29 (2021) 636–639.
[16] G. Katsuumi, I. Shimizu, M. Suda, Y. Yoshida, et al., Eur. Heart J. 41 (2020) 3746.
[17] S.H. He, N.E. Sharpless, Cell 169 (2017) 1000–1011.
[18] A. Hernandez-Segura, J. Nehme, M. Demaria, Trends Cell Biol. 28 (2018) 436–453.
[19] C.D. Camell, M.J. Yousefzadeh, Y. Zhu, et al., Science 373 (2021) 47.
[20] X. Li, W. Qiu, J. Li, et al., Chem. Sci. 11 (2020) 7292–7301.
[21] Y. Su, B. Yu, S. Wang, H. Cong, Y. Shen, Biomaterials 271 (2021) 120717.
[22] Y.L. Qi, H.R. Wang, L.L. Chen, et al., Coord. Chem. Rev. 445 (2021) 214068.
[23] L. Fu, Y. Tan, Y. Ding, W. Qing, Y. Wang, Chin. Chem. Lett. 35 (2024) 108886.
[24] Z. Wang, J. Li, J. Chen, et al., Chin. Chem. Lett. 34 (2023) 108507.
[25] R. Chen, W. Li, R. Li, et al., Chin. Chem. Lett. 34 (2023) 107845.
[26] L. Wu, J. Liu, P. Li, B. Tang, T.D. James, Coord. Chem. Rev. 50 (2021) 702–734.
[27] J. Krämer, R. Kang, L.M. Grimm, et al., Chem. Rev. 122 (2022) 3459–3636.
[28] J. Huang, K. Pu, Angew. Chem. Int. Ed. 59 (2020) 11717–11731.
[29] L.V. Wang, S. Hu, Science 335 (2012) 1458–1462.
[30] L.L. Zeng, G.C. Ma, J. Lin, P. Huang, Small 14 (2018) 18.
[31] Y. Wu, S. Huang, J. Wang, et al., Nat. Commun. 9 (2018) 3983.
[32] R.S. Mezrich, Radiology 291 (2019) 50–51.
[33] Z.X. Zhao, C.B. Swartchick, J. Chan, Chem. Soc. Rev. 51 (2022) 829–868.
[34] E. Fitsiou, A. Soto-Gamez, M. Demaria, Semin. Cancer Biol. 81 (2022) 5–13.
[35] S. Wang, B. Zhu, B. Wang, et al., Chin. Chem. Lett. 32 (2021) 1795–1798.
[36] D. Ma, S. Hou, C. Bae, et al., Chin. Chem. Lett. 32 (2021) 3886–3889.
[37] J.C. Acosta, J. Gil, Trends Cell Biol. 22 (2012) 211–219.